PAPER

Mirror-coupled plasmonic nanostructures for enhanced in-plane magnetic dipole emission

IOP Publishing Journal of Physics D: Applied Physics
J. Phys. D: Appl. Phys. **58** (2025) 015101 (11pp) https://doi.org/10.1088/1361-6463/ad7d9d

Mirror-coupled plasmonic nanostructures for enhanced in-plane magnetic dipole emission

Ruizhao Yao, Sheng Lan and Guang-Can Li*

Guangdong Provincial Key Laboratory of Nanophotonic Functional Materials and Devices, School of Information and Optoelectronic Science and Engineering, South China Normal University, Guangzhou, People's Republic of China

E-mail: guangcan.li@m.scnu.edu.cn

Received 9 June 2024, revised 18 August 2024
Accepted for publication 20 September 2024
Published 14 October 2024

Abstract

Self-assembling of plasmonic nanoparticles into an oligomer can produce optical nanoantennas with resonant magnetic responses, which constitutes a promising platform to study magnetic light-matter interactions at the nanoscale. However, these self-assembled magnetic nanostructures typically feature a flat-lying geometric configuration, giving rise to out-of-plane magnetic dipole (MD) moments that cannot couple to the far-field light efficiently. Herein, we propose a new geometric configuration of plasmonic nanoantennas to realize in-plane MD responses. This is achieved by elegantly coupling a plasmonic nanoparticle oligomer to one or more adjacent metal mirrors, virtually forming a vertically standing nanoparticle tetramer or trimer, yet with in-plane MD moments. We verified this design strategy by numerically simulating the resonance responses of three typical mirror-coupled nanostructures, all exhibiting pronounced resonant MD characters. Furthermore, optical magnetic emitters can be readily coupled to these plasmonic nanoantennas and gain an emission enhancement of two orders of magnitude while simultaneously featuring a high emission directionality (collection efficiency up to $\sim 70\%$ evaluated with common microscopy optics). We believe these mirror-enabled magnetic nanoantennas could lead to novel nanophotonic devices fully exploiting the magnetic nature of light.

Supplementary material for this article is available online

Keywords: magnetic dipole responses, surface plasmon resonances, plasmonic nanostructures, in-plane magnetic resonances

1. Introduction

Nanostructured materials can produce significant optical magnetic responses that rarely exist in nature, which enables a practical way to create building blocks for negative-index metamaterials and versatile metasurfaces [1, 2]. These artificial optical magnetic nanostructures can also accommodate emitters having optical magnetic dipole (MD) transitions to boost light emission processes via the so-called Purcell effect [3, 4], significant for many advanced photonic applications such as quantum single photon sources, nanolasers, ultrafast optoelectrical switches, and more [5].

To efficiently boost MD light emission using an artificial magnetic nanostructure, it requires the emitters to be precisely positioned at the magnetic field 'hot spot' of a host structure [3, 6], a nanometric volume in which magnetic fields are trapped. In the past decade, high-index dielectric nanoparticles

* Author to whom any correspondence should be addressed.

(silicon, gallium arsenide, etc) have been recognized as the most promising artificial magnetic nanomaterials, due mainly to their strong resonant magnetic responses and low optical loss in the visible to near-infrared range [2, 7]. Nevertheless, their magnetic modal fields are mainly confined inside the constituent materials [8], thereby inaccessible to external magnetic emitters. Merely placing magnetic emitters close to a dielectric nanoantenna does not ensure strong coupling interactions for a significant MD emission enhancement [9, 10]. Although some studies have proposed the design of hollow dielectric nanoparticles or voids-in-dielectric structures to expose magnetic modal fields to air [11–14], the practical structure fabrication is difficult, and precisely loading MD emitters to small magnetic hot spots remains challenging [15].

Another kind of artificial magnetic nanomaterial are metal nanostructures showing resonant magnetic-type plasmonic responses, such as the well-known split ring resonators (SRRs) [16, 17] and ring-shaped nanoparticle clusters (trimers, tetramers, etc) [18–24]. In contrast to their dielectric counterparts, these metallic plasmonic nanostructures strongly confine magnetic fields in nanometric gaps, accessible to external MD emitters. Two mechanisms that account for the magnetic responses of these metal nanostructures: the lumped inductor–capacitor resonator [16] initially proposed to describe the magnetic behavior of single SRRs, and the electric displacement current loop model [25], which defines an MD source responsible for the magnetic scattering resonances of ring-shaped nanoparticle clusters. While the SRRs' magnetic resonances are limited to the microwave and infrared range [26, 27], the ring-shaped nanoclusters could give rise to magnetic resonances in the visible and near-infrared ranges, thus allowing resonant coupling to be naturally available magnetic emitters with optical transitions, for example, the rare earth ions (e.g. Eu^{3+}) [28, 29]. Despite the non-negligible optical loss of plasmonic metals, the much smaller mode volumes of metal magnetic nanoantennas promise strong magnetic Purcell enhancement comparable to or even stronger than their dielectric counterparts [30–32].

So far, optical magnetic plasmonic nanoantennas have been fabricated either with lithographic methods [16, 17, 33, 34], or by self-assembling of metal nanoparticles [18, 20, 35, 36], both yielding nanostructures in a flat-lying arrangement (see upper panel in figure 1). Individually, such planar structural arrangement produces a flat-lying electric displacement current loop upon optical excitation, which defines an MD nanoantenna with a vertically oriented (out-of-plane) dipole moment. This out-of-plane MD nanoantenna scatters incident light or locally generated photons into high polar angle directions, which is not favorable for far-field detection and thereby practical spectroscopy applications.

Here, we propose a design strategy for plasmonic nanoantennas with in-plane MD responses, by employing so-called mirror-coupled metal nanostructures [37–39]. The basic idea is that individual metal nanostructures together with their images induced in mirrors forms a virtual vertically standing ring-shaped nanocluster (figure 1). These virtual nanoclusters should exhibit MD responses similar to the real ones, but with in-plane dipole moments. We demonstrated this design strategy by three representative structure configurations: (1) a metal nanosphere dimer atop a mirror, forming a virtual nanotetramer (VNT4, figure 1(a)), (2) a virtual nanotrimer (VNT3, figure 1(b)) comprised of a nanoparticle monomer coupled to its two images in two angled mirrors and (3) another virtual nanotetramer (VNT4′, figure 1(c)) different from VNT4, formed from a particle monomer closely spaced from three adjacent mirrors. Electromagnetic simulation results confirm the in-plane MD responses of these three constructs and reveal strong magnetic field confinement in their metal nanogaps. MD emitters can be readily loaded into these nanogaps, producing large MD emission enhancements with a Purcell factor of up to 1200 while simultaneously attaining a high collection efficiency of $\sim 70\%$ using common microscope optics.

2. Results and discussion

2.1. The working principle for mirror-coupled metal nanoparticles generating in-plane MD responses

Our design strategy for the in-plane magnetic nanoantenna is inspired by the well-known nanoparticle-on-mirror (NPoM) construct [39–41], which behaves like a vertically oriented nanoparticle dimer. Within the dipole approximation, the nanoparticle in a NPoM structure can be seen as a particle dipole. Following the electromagnetic image theory in classic electrodynamic textbooks, this particle dipole induces charges in the underlying mirror, creating an image dipole orientated vertically or transversely depending on the dipole excitation orientation. Therefore, the optical response of a NPoM structure can be equivalently described by a vertically aligned nanoparticle dimer.

In a similar way, we can replace the nanosphere monomer in single NPoM constructs with a nanodimer, hopefully creating a virtual nanotetramer exhibiting MD resonances like a real nanotetramer (RNT4) [21, 22, 42], as shown in figure 1(a). Being different from the flat-lying RNT4 (upper panel in figure 1(a)), this VNT4 is comprised of a nanosphere dimer and its image induced by the underlying mirror, defining a nanotetramer rotated by 90° with respect to the flat-lying RNT4 and so did its MD moment, i.e. $m_z \rightarrow m_y$. Inspired by the significant MD responses of a real nanotrimer (RNT3) [19, 20, 43], we can also replace the flat mirror in single NPoM constructs with a V-shaped one to create a virtual nanotrimer (bottom panel in figure 1(b)). The VNT3 is formed from the nanoparticle monomer and its two images in the angled mirrors, which should behave like a real nanotrimer (inset in figure 1(b)) but is rotated by 90° with respect to the flat-lying RNT3 (upper panel in figure 1(b)). Similarly, three adjacent mirrors together with a nearby nanoparticle monomer form another configuration of the virtual nanotetramer, as shown in figure 1(c) (bottom panel). The real particle induced three images in the nearby mirrors and together with itself defines a vertically standing nanotetramer featuring an in-plane MD moment.

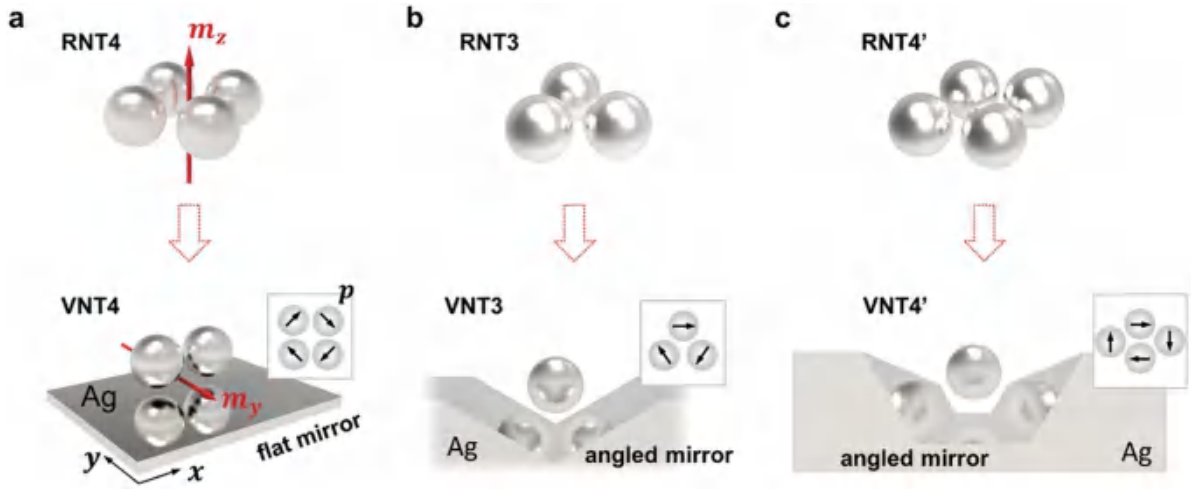

Figure 1. Schematic illustration of the formation of a magnetic nanoantenna with mirror-coupled metal nanostructures. (a) A silver nanosphere dimer together with its image in a flat mirror forms a virtual nanotetramer (VNT4, lower panel). In contrast to the flat-lying real-nanotetramer (RNT4, upper panel) exhibiting an out-of-plane magnetic dipole (MD) moment (m_z), this VNT4 features an in-plane MD moment (m_y) originating from the particle dipoles (p) and their images in mirror. Inset in the bottom panel shows the equivalent electromagnetic structure of a VNT4, for which p denotes the electric dipoles collectively forming the circulating displace current of a magnetic dipole source. (b) A silver nanosphere monomer together with its images in angled mirrors forms a virtual nanotrimer (VNT3, bottom panel), which behaves like a vertically standing nanotrimer with in-plane MD response (inset in bottom panel). The real nanotrimer with a flat-lying manner showing out-of-plane magnetic dipole moment (m_z) was also provided for reference (upper panel). (c) Another geometric configuration of a VNT4, labeled as VNT4′, formed from a nanosphere monomer and its images induced in three adjacent mirrors.

2.2. The plasmonic mode characters of the three mirror-coupled plasmonic nanostructures

To validate their in-plane MD response, we performed three-dimensional full-wave electromagnetic simulations using the commercially finite-element-method package by COMSOL Inc. The dielectric constant of silver was interpolated from experimental data [44]. For simplification, all the particle-particle and particle-mirror gap contents were set as air and, if not specifically stated, all the gap sizes were 1 nm and the nanosphere diameter was 80 nm. To ensure a robust iteration convergence in simulation, a mesh size of 1 nm and 0.2 nm were set for the nanoparticle volumes and the gap regions, respectively (for more details, see figure S1).

Figure 2(a) shows the simulated scattering responses of single VNT4 under plane wave illumination. When the incidence polarization is set along the dimer axis (s-polarized), a pronounced plasmon resonance peak appears at around 720 nm. This resonance vanishes when the polarization direction switches orthogonal to the dimer axis (p-polarized). To confirm whether this plasmon resonance is an MD mode, we calculated the near field distribution at this resonance wavelength. As shown in figure 2(b), the magnetic near-field intensity distribution exhibits a well-defined triangle-shaped 'hot spot' area, indicating strong confinement of magnetic fields. These strongly confined magnetic fields are dominated by the in-plane component (H_y figure S3), which induces a vortex electric field around the 'spot hot' region. Figure 2(c) shows the simulated three-dimensional surface charge distributions at the VNT4 resonance. It reveals a circulating electric displacement loop formed from the electric dipoles (ED) induced in both nanoparticles (p_1, p_2, see figure 2(d)) and the flat mirror (p_m), a near-field characteristic indicative of an MD source. It is worth noting that the tilted dipoles p_1 and p_2 cannot be induced by the electric field component (E_x) of incident light, otherwise they would be oriented colinearly and parallel to the direction of incident electric polarization (E_x). This is further confirmed by the fact that the MD-like VNT4 resonance responds dominantly to the magnetic field component of incident light, as discussed later (figure 3(a)). Based on these near-field characters, the formation of the MD resonance of individual VNT4 can be described by

$$p_1 + p_2 + p_\mathrm{m} \rightarrow m \tag{1}$$

where m is the induced MD moment. Following the dipole-image model, the charge dipoles induced in the mirror can be viewed as the sum of two nanoparticle dipole images (p_1',p_2', figure 2(d)), i.e.

$$p_\mathrm{m} = p_1' + p_2' \ . \tag{2}$$

Substituting this into equation (1), we obtain

$$p_1 + p_2 + p_1' + p_2' \rightarrow m \ . \tag{3}$$

Such a closed head-to-tail dipole arrangement has also been resolved in a real nanosphere tetramer although in a flat-laying manner [21, 22]. This similarity suggests that mirror-coupled nanosphere dimers indeed behave like real nanotetramers but with in-plane MD responses.

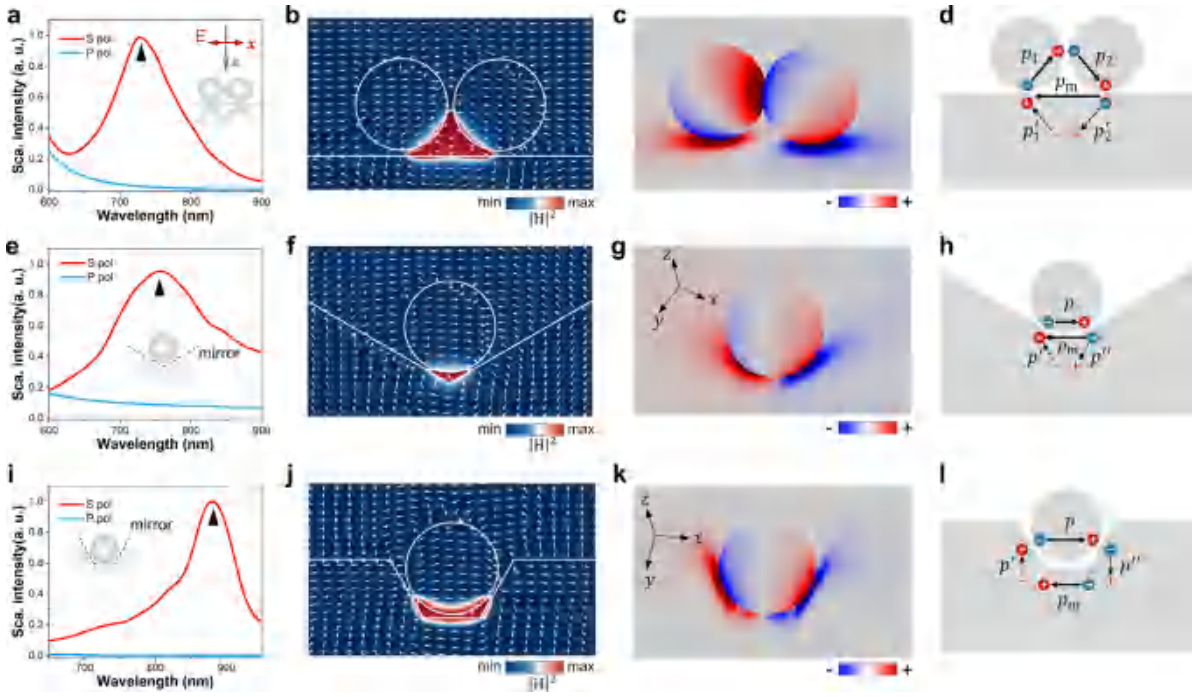

Figure 2. Magnetic resonance of single virtual tetramer and trimer nanoantenna. (a) Simulated scattering spectra of single VNT4, illuminated with S- (along x-axis) or P- (along y-axis) polarized plane wave. (b)–(c) Magnetic near-field intensity (b) and surface charge (c) distributions calculated at the MD resonance wavelength marked in (a). The white unit vectors overlapping with the magnetic field distributions in (b) represent the local electric field orientations. (d) Schematic illustration of the structural MD source induced in a VNT4 structure, showing the formation of a closed current loop via electric dipole coupling, the same scenario as for a real nanotetramer. (e)–(h) Similar results as (a)–(d) but for a single VNT3 structure. (i)–(l) Similar results as (a)–(d) but for a single VNT4′ structure.

Next, we simulated the plasmonic responses of single VNT3 structures with a mirror angle of 120°. The scattering spectrum, shown in figure 2(e), exhibits a broad plasmon resonance at around 750 nm when the magnetic field component of the incident plane-wave is oriented parallel to both mirror surfaces, i.e. H_y. Near-field calculations at the VNT3 resonance wavelength show that this resonant mode induces strong magnetic near-field localization in the closed gap region, along with a clear electric field vortex around it (figure 2(f)). The corresponding surface charges distribution reveals that the charges are mainly concentrated at the particle-mirror junctions (figure 2(g)). These near-field characters are in line with the predictions by the dipole-image model, which views a single nanoparticle coupled to the angled mirrors as a nanotrimer, formed from the particle dipole and its two images induced in the mirrors. Like a real nanoparticle trimer, the optical induction of the nanoparticle dipole (p) and its two images (p', p'') oriented in a head-to-tail manner form an electric displacement current loop (figure 2(h)), thereby defining an MD source as

$$p + p' + p'' \rightarrow m \ . \tag{4}$$

The single VNT4′ structures exhibit similar resonant MD response as the VNT3 and VNT4. As shown in figures 2(i) and (a) pronounced plasmon resonance can be identified at around 870 nm, associated with a strong magnetic field confinement in the closed central gap (figure 2(j)). In the same way, the formation of this magnetic-type mode can be attributed to the coupling between the nanoparticle dipole and its images (p', p'' and p''') induced in the three adjacent mirrors (figure 2(l)), read as

$$p + p' + p'' + p''' \rightarrow m \ . \tag{5}$$

2.3. Confirming the mode nature of the magnetic nanoantennas by inspecting their excitation responses

The plane-wave illumination configuration employed in figure 2 contains simultaneous electric and magnetic field components which allow excitations of both electric- and magnetic-type plasmon modes. To further confirm that the mode characters shown in figure 2 indeed originate from the excitation of in-plane MD modes, we inspected their excitation response to both the electric and magnetic components of incident light. To this end, in simulations we used a focused Gaussian beam to illuminate the above single nanostructures and evaluated their site-dependent absorption intensities at the resonance wavelengths by scanning the individual nanostructures through the beam focus (as depicted in figure 3(a)). The electric field polarization of the incident Gaussian beam is set along x (i.e. E_x) and the accompanying magnetic field is H_y. We calculated the electromagnetic field intensity distributions in the focal plane (see insets in figures 3(b) and (c), of which the line-cut profiles along both the x and y axis is shown in

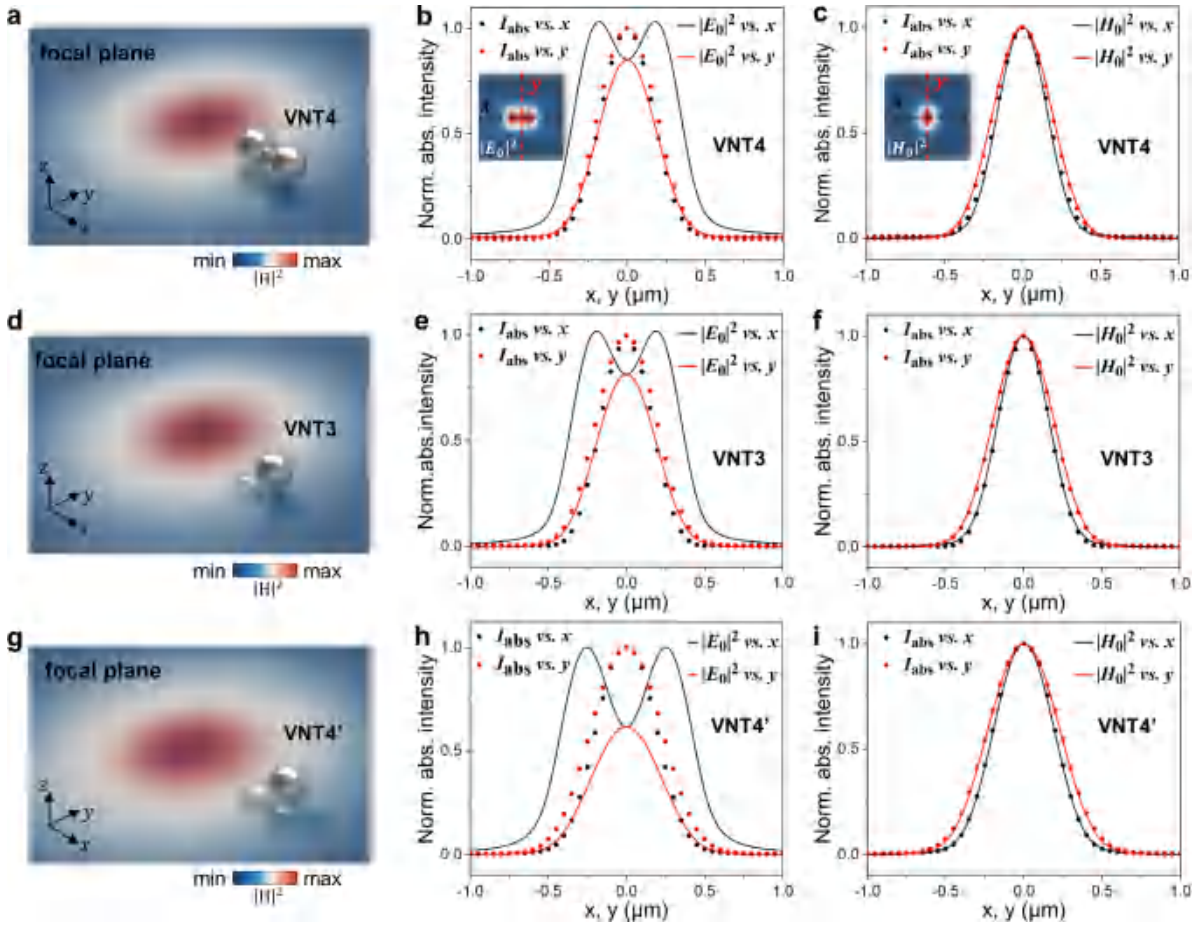

Figure 3. Excitation responses of single MD nanostructures. (a) Schematics of single VNT4 nanoantenna scanning through a focused Gaussian beam. The rendered backgrounds represent the magnetic field distributions in the focal plane of a focused Gaussian beam. The numerical aperture (NA) of the focusing lens is 0.9. (b) Comparison of the absorption intensities vs. *x*,*y* (dots) and the focal electric ($|E_0|^2$) intensities vs. *x*, *y* (solid line), calculated for single VNT4 scanning along the *x* or *y* axis. Inset shows the electric field distribution at the beam focus. These scanning absorption profiles are simulated at the resonant wavelengths as marked in figure 2 (black triangles). (c) Comparison of the VNT4 absorption intensities vs. *x*,*y* (dots) and the focal magnetic ($|H_0|^2$) intensities vs. *x*, *y* (solid line). Inset shows the magnetic field distribution at the beam focus. (d)–(f) Similar results as (a)–(c) but calculated for a VNT3 scanning through the same beam focus. (g)–(i) Similar results as (a)–(c) but calculated for a VNT4′ scanning through the same beam focus.

figure 3(b) (for the electric component $|E_0|^2$, solid curves) and figure 3(c) (for the magnetic component $|H_0|^2$, solid curves). To excite the magnetic-like resonances, the MD moment of individual nanostructures are aligned to the magnetic field polarization of the excitation light, for instance, the VNT4 with dimer axis oriented orthogonal to the dominant magnetic field (H_y, see figure 3(a)) of employed Gaussian beam. Each nanostructure scanning the beam focus will behave as a nanoprobe to map the electric or magnetic field of excitation light, depending on the excited mode nature.

The site-dependent absorption intensities of an individual VNT4, VNT3, or VNT4′ moving along both the *x* and *y* axis was calculated and compared to the electric and magnetic field intensity distributions along these scanning paths. For single VNT4 nanostructures, it was found that the normalized absorption intensity (I_{abs}) *vs.* *x* or *y* (dotted lines in figure 3(c)) perfectly follow the line profiles of focal magnetic field intensity along the same scanning path (solid lines in figure 3(c)) but significantly deviates from the electric field distribution profiles (solid lines in figure 3(b)). This suggests that the nanoprobe absorption at the illumination wavelength is dominantly driven by the magnetic field of the excitation light, a key characteristic indicative of the magnetic mode nature. We observed similar results when scanning the same beam focus with a single VNT3 ((figure 3(d))) and VNT4′ (figure 3(g)), both showing excellent agreement between the mapped absorption profiles (I_{abs} *vs.* *x*, *y*) and the focal magnetic field distributions ($|H_0|^2$ *vs.* *x*, *y*, see figures 3(f) and (i)). In addition, figure 3(e) and h showed marked discrepancies between the profiles of I_{abs} *vs* *x*, *y* and that of the focal electric field distribution ($|E_0|^2$ *vs.* *x*, *y*) for both VNT3 and VNT4′, indicating their negligible response to the electric field of excitation light.

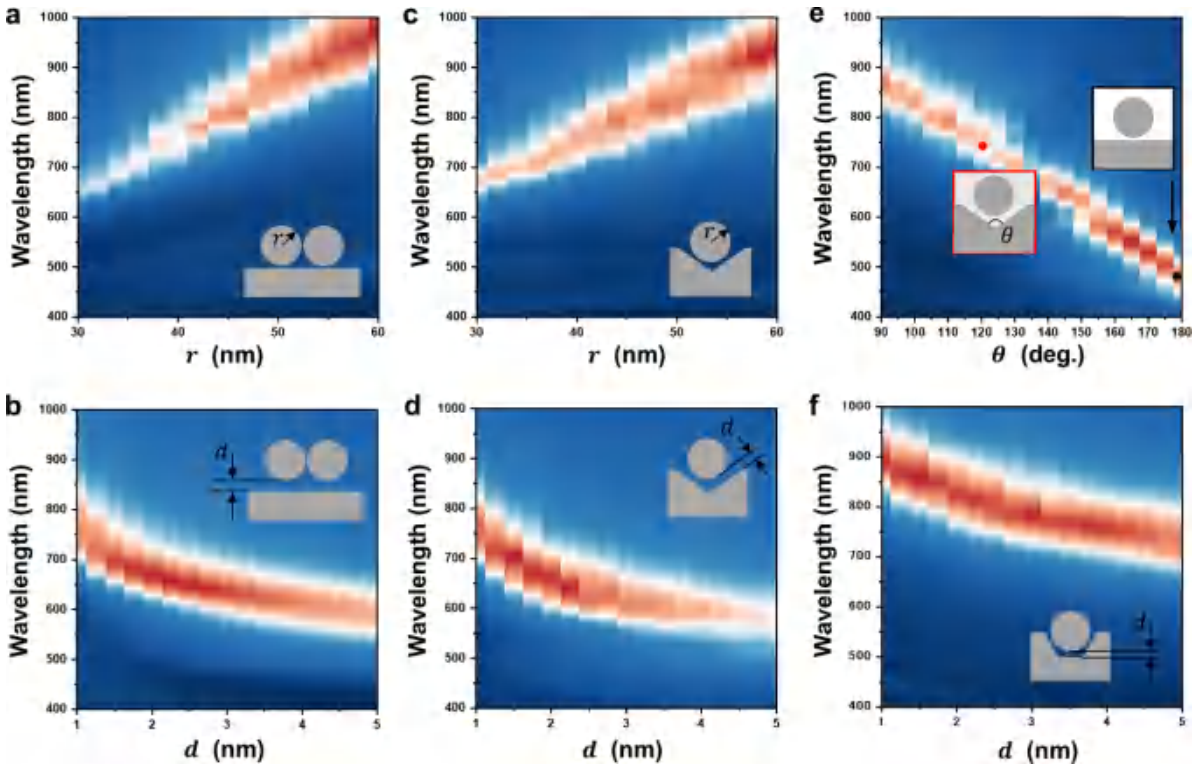

Figure 4. Scattering MD resonance evolutions of single virtual tetramer and trimer nanostructures with varying geometric sizes and configurations. (a), (b) Nanoparticle size (a) and gap distance (b) dependent MD resonances of single VNT4 nanoantenna. The particle-particle gap distance was fixed at 1 nm and the particle diameter is 80 nm unless otherwise noted. (c), (d) Similar results as (a), (b) but for a VNT3 structure. (e) Mirror angle dependent MD resonance of single VNT3 antenna. (f) Gap distance dependent MD resonances of single VNT4′.

2.4. The magnetic resonance evolution with varying geometric parameters

Electromagnetic resonances in plasmonic nanostructures are sensitive to their geometric parameters. We numerically study the dependence of the magnetic plasmon resonances of individual VNT4 and VNT3 on the nanoparticle and gap sizes. As shown in figure 4, both the VNT4 (figure 4(a)) and VNT3 (figure 4(c)) resonances monotonically red shift with increasing nanoparticle sizes. This trend of reduced resonance energy for larger metal nanoparticles can be ascribed to their increased dipole moments, which result in higher radiation losses. The gap distances between nanoparticles and mirrors strongly affect the near-field coupling strengths and therefore the MD resonances. For both the VNT4 and VNT3 structures, decreasing the nanoparticle-mirror gap distances significantly redshifts the MD resonance wavelengths, and simultaneously, the resonance line widths get wider (figures 4(b) and (d)). In contrast to the narrowing of the ED resonances typically observed for plasmonic nanoparticles approaching a mirror [45, 46], this linewidth broadening effect of an MD resonance can largely be attributed to the increased weight of the MD component among the various multiple contributions at this resonance (see further discussions in figures S5 and S6).

It should be noted that our numerical simulations are based on the classical electrodynamic model and are not able to capture the MD characters of the above nanostructures with gap sizes below 1 nm. This is because the quantum tunneling (QT) effect would come into play at the sub-1 nm scale [47, 48]. The occurrence of QT will short out the metal gaps and thus weaken the MD resonances [19]. In the extreme situation, the MD resonances vanish when the facing gap surfaces of the particle-particle (figure S7) or particle-film nanojunctions get in touch with each other [49]. We also examine the dependence of the VNT4 resonances on the mirror angles. As shown in figure 4(e), the VNT3 resonances monotonically blue shift with increasing mirror angles. At an angle of 180°, the two nanoparticle images in the mirrors merge into one, forming the well-known NPoM configuration [39]. The corresponding NPoM resonance, although showing magnetic near-field confinement in the gap region (figure S9(a)), is an electric quadrupole (EQ)-like hybrid mode originating from the transverse bonding of a horizontally oriented nanoparticle dipole and its image in a flat mirror [50]. This is further corroborated by the calculated surface charge distributions shown in figure S9(b) and particularly, the absorption profile of a NPoM scanning across a vectorial light beam (figure S9(d)), which shows that the NPoM resonance is dominantly driven by the electric field of the excitation light. Meanwhile, we would like to emphasize that plasmon resonances with a single magnetic near-field hot spot may not be magnetic modes. In particular, in some plasmonic nanoantennas comprised of two coupled elements

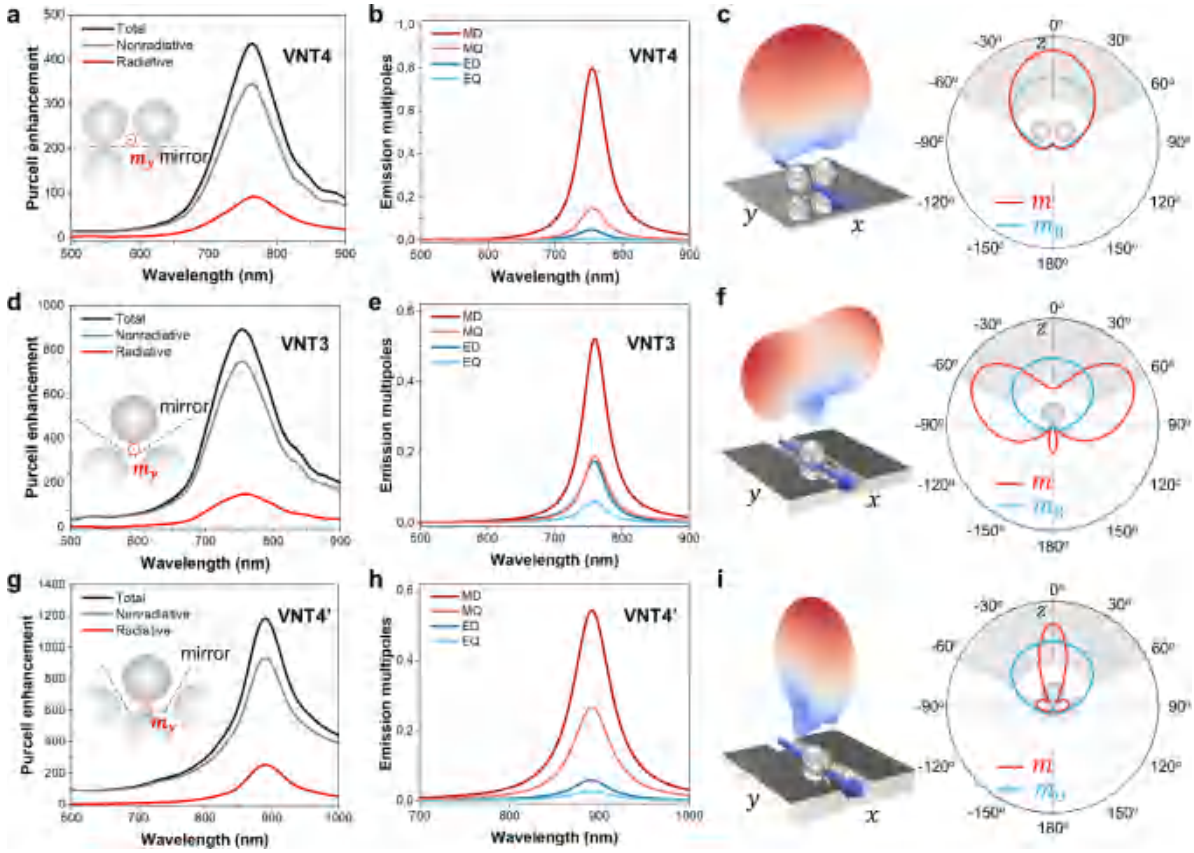

Figure 5. Enhancement of magnetic dipole emission by single VNT4 and VNT3 structures. (a) Purcell enhancement of single VNT4-coupled magnetic dipole. The MD source is placed at the center of the triangular gap region enclosed by the two nanoparticles and mirrors, and its dipole moment is aligned with the local magnetic field (H_y) for strongest coupling interaction. (b) Multipole expansion of emission from the VNT4-coupled MD source in (a), which helps to evaluate the contribution of the different modes to the total emission. (c) The far field radiation pattern of the VNT4-coupled MD source. The polar plotting shows the angular intensity distribution in the *xz* plane. The polar emission profile of a *y*-oriented magnetic dipole emitter atop a mirror is also provided for reference (blue curve). The shadowed region corresponds to the collection range of an objective with a numerical aperture of 0.9. (d)–(f) Similar results as (a)–(c) but for a VNT3-coupled MD source. (g)–(i) Similar results as (a)–(c) but for a VNT4′-coupled MD source. All the structural parameters employed in simulations are identical to that in figure 2

[25, 51], the EQ-like resonance associated with an anti-parallel dipole configuration shows a similar magnetic near-field profile as an MD mode but responds dominantly to the electric field of excitation light, for example, the metal–insulator–metal and nanoparticle monomers on mirror structures [50, 52].

2.5. Evaluation of the magnetic Purcell enhancement by the three magnetic nanoantennas

To evaluate the magnetic Purcell enhancement in the above MD nanoantennas, we use single MDs to mimic a point emitter with optical MD transitions and position it at the magnetic field 'hot spot' of single virtual tetramers and trimers (insets in figures 5(a), (d) and (g)). The Purcell Factor (F_P), defined as the ratio of the dipole transition decay rate in a modified electromagnetic environment (γ) to that in vacuum (γ_0), was used to characterize the modification of the emitter transition by a nanoantenna. In a phenomenological way, the F_P can be calculated by evaluating the ratio of the dipole source power with the nanoantenna at present or not, i.e. $F_P = \gamma/\gamma_0 = P/P_0$, where P is the antenna-modified dipole power and P_0 denotes the emission power of a dipole in vacuum space. In our simulation, the dipole moment of single MD emitters was set so as to be aligned to the local magnetic fields (H_y) to achieve optimized coupling to the structural MD modes. Figures 5(a), (d) and (g) show wavelength-dependent F_P calculated respectively for the above single nanoantennas. All the nanostructures exhibit maximal F_P at their scattering resonance wavelengths, indicating unambiguously the dominant role of structural MD resonances in the Purcell enhancement effect. Compared to an MD emitter in vacuum, the transition decay of a dipole optimally coupled to a VNT4 antenna can be accelerated by a factor of ~ 450 (figure 5(a)), significantly surpassing the typical high-index dielectric nanoantennas [12, 13, 53]. The magnetic Purcell enhancement is more pronounced for the VNT3 antenna, which exhibits an F_P up to ~ 900 at the MD resonance wavelength (figure 5(d)). Stronger Purcell enhancement was demonstrated by loading a point MD emitter into the gap of a VNT4′ (figure 5(g)), with a F_P

of ~ 1200, comparable to the highest F_P achievable in low-loss dielectric nanoantennas [54]. Nevertheless, metal-based plasmonic nanoantennas suffer significant Ohmic loss, which renders only a small fraction of the total dipole energy radiating into free space. We evaluated the radiation efficiencies (η) of these MD emitter-coupled nanoantennas using $\eta = P_{rad}/P$, where P_{rad} is the net dipole power radiated into free space. The calculation results showed a $\eta \sim 21\%$ for single VNT4, $\eta \sim 17\%$ for single VNT3 and $\eta \sim 22\%$ for single VNT4′ at their respective resonance wavelengths are all relatively low with respect to their dielectric counterparts [12, 13]. Despite this, the radiative Purcell factor, defined as $F_{rad} = P_{rad}/P_0 = \eta F_P$, is remarkably high, with a F_{rad} of ~ 96 (figure 5(a)) for a VNT4, ~ 153 for a VNT3 and ~ 258 for a VNT4′ (figure 5(c)). This means that the emission of these magnetic nanoantenna-coupled MD emitters can be enhanced by an averaged two orders of magnitude with respect to that in vacuum, significant for enhancement of diverse spectroscopy applications.

The coupling of MD emitters to the above nanoantennas not only boosts their emission rate but also modifies their far-field radiation characters. Based on a near-to-far field transformation frame [55], we calculated the angular emission distribution of an MD coupled to single VNT4 antennas. As depicted in figure 5(c), the VNT4 exhibited a peach-shaped emission pattern, with the majority of the radiation energy directed upward. Such a directional emission pattern is favorable for optical spectroscopy because it enables efficient collection of the emission with common microscope objectives. Our calculation results showed ∼66% of the emission from a VNT4-coupled MD source can be captured using an air objective with a moderately numerical aperture (NA = 0.9, figure 5(c)). This is in sharp contrast to flat-lying plasmonic MD nanoantennas, say, SRRs, real nanotetramers and trimers, which feature out-of-plane MD responses and scatter the emission of coupled MD sources in lateral directions, giving rise to collection efficiencies typically lower than $\sim 30\%$ (see figure S10). In the same way, we calculated the emission pattern of a VNT3-coupled MDs source. As depicted in figure 5(f), the VNT3 emission profile exhibits splitting intensity maxima at angles markedly deviated from the substrate norm direction. This two-lobe shaped emission pattern results in reduced collection efficiency ($\sim 53\%$) with respect to the VNT4 antenna. We attribute the distinct emission characters of VNT4- and VNT3-coupled MD sources to their different mode natures. Figure 5(b) shows the different multipole mode components contributing to the total emission of a VNT4-coupled MD, calculated with a modified multipole expansion method described in [56]. The results reveal that the MD mode component dominates the total emission, suggesting that the presence of a VNT4 structure marginally modifies the emission character of an MD emitter, while simultaneously enabling a large emission enhancement. This is also in line with the emission patterns of VNT4-coupled MD emitters, which show similar angular emission profiles to that of a bare in-plane MD atop the metal surface (figure S12). Cutting off the total emission components to the four lowest-order multipole modes, we define a factor δ to characterize the MD mode purity of the nanoantenna-coupled MD sources by

$$\delta_{md} \approx \frac{P_{md}}{P_{md}+P_{ed}+P_{mq}+P_{ed}} \tag{6}$$

where P_{md}, P_{ed}, P_{mq}, and P_{ed} corresponds to the emission power of the MD, ED, magnetic quadrupole (MQ), and EQ modes, respectively. These gives rise to a $\delta_{md} \sim 0.8$ for the VNT4 at the MD resonance wavelength, indicating a high-purity MD mode nature. In contrast, the VNT3 enhanced emission contains considerable ED ($\delta_{ed} \sim 0.21$) and MQ ($\delta_{mq} \sim 0.19$) mode components (figure 5(e)). The interference between these concurrent modes smear the far-field profile of the dominant MD emission mode ($\delta_{md} \sim 0.52$) and thereby slightly weakening its radiation directionality. For the VNT4′ coupled MD emitters, the contribution of the MQ component becomes significant (figure 5(h)). This results in a different emission pattern with respect to the VNT4 and give rises to a higher collection efficiency up to $\sim 70\%$ (figure 5(i)).

2.6. Transformation of electric-type dipole emission to a magnetic-type one by the magnetic plasmonic nanoantennas

One key advantage of mirror-coupled plasmonic nanoantennas is that optical emitters can be readily embedded into the particle-mirror gaps in a layered manner using well-established layer deposition and molecular self-assembling methods [57, 58]. In practice, the MD transitions of optically magnetic emitters are often accompanied by ED transitions [28]. When loading an emitter layer on the mirror surfaces, not only the MD transitions are boosted at the magnetic field 'hot spots' but also the ED transitions at the electric field 'hot spots' could be excited (figure 6). In experimental implementation, this may lead to mixed excitations and hybrid emission responses dressed by significant electronic characteristics. To evaluate this effect, we expanded the emission multipoles of an ED source residing at the VNT4 particle-mirror nanojunctions. As shown in figure 6(a), this local ED source is found to exhibit pronounced MD emission characters, with a $\delta_{md} \sim 0.76$ at the structural MD resonance wavelength. Similar observations were made for the VNT3 and VNT4′ nanoantennas respectively coupled to an ED source in the nanoparticle-mirror gaps (see figures 6(b) and (c)), with the former exhibiting a $\delta_{md}$of ~ 0.53 and the latter showing a $\delta_{md}$of ~ 0.62 at their MD resonance wavelengths. Together with the results shown in figure 5, it can be concluded that the mirror-enabled virtual tetramer and trimer nanoantennas not only amplify the emission of locally coupled MD sources but also behave like an optical transducer capable of transforming an electric-type emission source into a magnetic one. This potentially opens a new way to achieve magnetic-type light sources that are currently limited to a few natural materials with magnetic optical transitions, but highly demanded for advanced metamaterial-based applications.

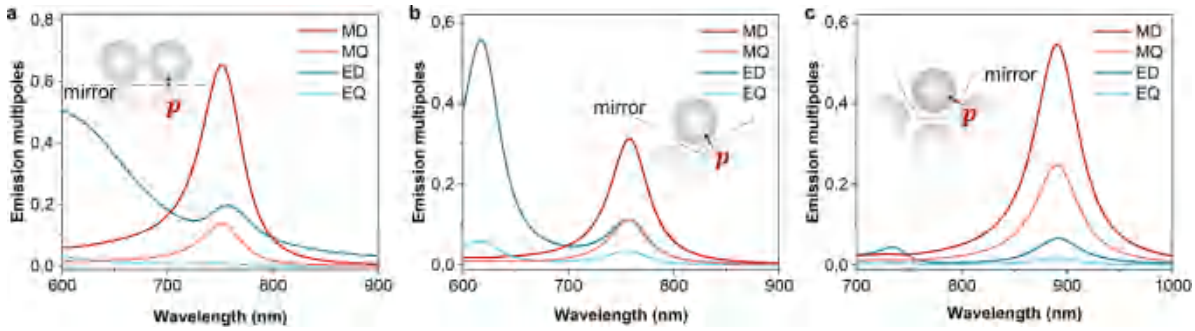

Figure 6. Transducing an optical ED source to a magnetic one via coupling to a single magnetic nanoantenna. (a) Multipolar expansion of emission from a VNT4 coupled ED source. The dipole moment of the ED source is aligned with the local electric fields (E_z) in the gap for strongest coupling. (b) Similar results as (a) but for a VNT3 structure. (c) Similar results as (a) but for a VNT4′ structure. All the structural parameters employed in simulations are identical to that in figure 2.

3. Conclusions

We have proposed a new geometric configuration of plasmonic nanoantennas to achieve resonant in-plane MD responses, formed from a metal nanoparticle monomer or oligomer closely coupled to one or multiple adjacent metal mirrors. Using full-wave electromagnetic simulations, we demonstrate three typical magnetic nanoantennas in this particle-mirror coupling configuration, all exhibiting pronounced MD mode characters in both the near-field and far-field scattering responses. Furthermore, we show that the emission of an MD emitter optically coupled to these magnetic nanoantennas can be enhanced by an averaged two orders of magnitude while simultaneously featuring high collection efficiencies with common microscopy optics (up to 70%). We anticipate that these structural configurations will also apply to other-shaped nanoparticles to achieve in-plane MD emission, say, in nanocubes (as demonstrated in figure S8). Compared to dielectric magnetic nanoantennas, these plasmonic nanostructures can readily accommodate emitters into their gaps, which provides not only a nanoscale playground to exploit the magnetic-type light-matter interactions but also an enhancement platform for advanced magnetic light spectroscopy.

Data availability statement

The data cannot be made publicly available upon publication because no suitable repository exists for hosting data in this field of study. The data that support the findings of this study are available upon reasonable request from the authors.

Acknowledgments

This work was financially supported by the National Natural Science Foundation of China (Grant No 12274147), the Natural Science Foundation of Guangdong Province (Grant No. 2023A1515012368), the Natural Science Foundation of Guangzhou (Grant No. 202201010445) and the International Academic Exchange Program of Guangdong Province (Grant No. 2022A0505030012).

Conflict of interest

The authors have no competing interests to declare that are relevant to the content of this article.

ORCID iDs

Ruizhao Yao https://orcid.org/0009-0008-2967-550X
Guang-Can Li https://orcid.org/0000-0002-9903-8900

References

[1] Wu Y, Xie P, Ding Q, Li Y, Yue L, Zhang H and Wang W 2023 Magnetic plasmons in plasmonic nanostructures: an overview *J. Appl. Phys.* **133** 030902
[2] Kuznetsov A I, Miroshnichenko A E, Brongersma M L, Kivshar Y S and Luk'yanchuk B 2016 Optically resonant dielectric nanostructures *Science* **354** aag2472
[3] Baranov D G, Savelev R S, Li S V, Krasnok A E and Alù A 2017 Modifying magnetic dipole spontaneous emission with nanophotonic structures *Laser Photonics Rev.* **11** 1600268
[4] Horvath S P *et al* 2023 Strong Purcell enhancement of an optical magnetic dipole transition (arXiv:2307.03022)
[5] Staude I, Pertsch T and Kivshar Y S 2019 All-dielectric resonant meta-optics lightens up *ACS Photonics* **6** 802–14
[6] Mignuzzi S, Vezzoli S, Horsley S, Barnes W L, Maier S A and Sapienza R 2019 Nanoscale design of the local density of optical states *Nano Lett.* **19** 1613–7
[7] Jahani S and Jacob Z 2016 All-dielectric metamaterials *Nat. Nanotechnol.* **11** 23–36
[8] Li G C, Xiang J, Zhang Y L, Deng F, Panmai M, Zhuang W, Lan S and Lei D 2021 Mapping the magnetic field intensity of light with the nonlinear optical emission of a silicon nanoparticle *Nano Lett.* **21** 2453–60
[9] Vaskin A *et al* 2019 Manipulation of magnetic dipole emission from Eu^{3+} with Mie-Resonant dielectric metasurfaces *Nano Lett.* **19** 1015–22
[10] Sugimoto H and Fujii M 2021 Magnetic Purcell enhancement by magnetic quadrupole resonance of dielectric nanosphere antenna *ACS Photonics* **8** 1794–800
[11] Yang Y, Zhu B, Dai H and Sun X 2019 Identical emission enhancement for arbitrary-orientation magnetic dipole emitters in silicon hollow nanocavity *Opt. Express* **27** 25931–25942

[12] Feng T, Xu Y, Liang Z and Zhang W 2016 All-dielectric hollow nanodisk for tailoring magnetic dipole emission *Opt. Lett.* **41** 5011
[13] Feng T, Zhang W, Liang Z, Xu Y and Miroshnichenko A E 2018 Isotropic magnetic Purcell effect *ACS Photonics* **5** 678–83
[14] Li J, Verellen N and Van Dorpe P 2017 Enhancing magnetic dipole emission by a nano-doughnut-shaped silicon disk *ACS Photonics* **4** 1893–8
[15] Matsumori A, Sugimoto H and Fujii M 2022 Silicon nanosphere with accessible magnetic hotspot *Adv. Opt. Mater.* **10** 2102574
[16] Linden S, Enkrich C, Wegener M, Zhou J, Koschny T and Soukoulis C M 2004 Magnetic response of metamaterials at 100 terahertz *Science* **306** 1351–3
[17] Klein M W, Enkrich C, Wegener M and Linden S 2006 Second-harmonic generation from magnetic metamaterials *Science* **313** 502–4
[18] Fan J A, Wu C, Bao K, Bao J, Bardhan R, Halas N J, Manoharan V N, Nordlander P, Shvets G and Capasso F 2010 Self-assembled plasmonic nanoparticle clusters *Science* **328** 1135–8
[19] Scholl J A, Garcia-Etxarri A, Aguirregabiria G, Esteban R, Narayan T C, Koh A L, Aizpurua J and Dionne J A 2016 Evolution of plasmonic metamolecule modes in the quantum tunneling regime *ACS Nano* **10** 1346–54
[20] Yeşilyurt A T M, Sanz-Paz M, Zhu F, Wu X, Sunil K S, Acuna G P and Huang J S 2023 Unidirectional meta-emitters based on the Kerker condition assembled by DNA origami *ACS Nano* **17** 19189–96
[21] Shafiei F, Monticone F, Le K Q, Liu X X, Hartsfield T, Alù A and Li X 2013 A subwavelength plasmonic metamolecule exhibiting magnetic-based optical Fano resonance *Nat. Nanotechnol.* **8** 95–99
[22] Barrow S J, Collins S M, Rossouw D, Funston A M, Botton G A, Midgley P A and Mulvaney P 2016 Electron energy loss spectroscopy investigation into symmetry in gold trimer and tetramer plasmonic nanoparticle structures *ACS Nano* **10** 8552–63
[23] Sheikholeslami S N, García-Etxarri A and Dionne J A 2011 Controlling the interplay of electric and magnetic modes via Fano-like plasmon resonances *Nano Lett.* **11** 3927–34
[24] Campione S, Guclu C, Ragan R and Capolino F 2014 Enhanced magnetic and electric fields via Fano resonances in metasurfaces of circular clusters of plasmonic nanoparticles *ACS Photonics* **1** 254–60
[25] Monticone F and Alù A 2014 The quest for optical magnetism: from split-ring resonators to plasmonic nanoparticles and nanoclusters *J. Mater. Chem.* C **2** 9059–9072
[26] Klein M W, Enkrich C, Wegener M, Soukoulis C M and Linden S 2006 Single-slit split-ring resonators at optical frequencies: limits of size scaling *Opt. Lett.* **31** 1259
[27] Zhou J, Koschny T, Kafesaki M, Economou E N, Pendry J B and Soukoulis C M 2005 Saturation of the magnetic response of split-ring resonators at optical frequencies *Phys. Rev. Lett.* **95** 223902
[28] Kasperczyk M, Person S, Ananias D, Carlos L D and Novotny L 2015 Excitation of magnetic dipole transitions at optical frequencies *Phys. Rev. Lett.* **114** 163903
[29] Taminiau T H, Karaveli S, Van Hulst N F and Zia R 2012 Quantifying the magnetic nature of light emission *Nat. Commun.* **3** 979
[30] Mivelle M, Grosjean T, Burr G W, Fischer U C and Garcia-Parajo M F 2015 Strong modification of magnetic dipole emission through diabolo nanoantennas *ACS Photonics* **2** 1071–6
[31] Hein S M and Giessen H 2013 Tailoring magnetic dipole emission with plasmonic split-ring resonators *Phys. Rev. Lett.* **111** 026803
[32] Feng T, Zhou Y, Liu D and Li J 2011 Controlling magnetic dipole transition with magnetic plasmonic structures *Opt. Lett.* **36** 2369
[33] Hentschel M, Dorfmüller J, Giessen H, Jäger S, Kern A M, Braun K, Zhang D and Meixner A J 2013 Plasmonic oligomers in cylindrical vector light beams *Beilstein J. Nanotechnol.* **4** 57–65
[34] Hentschel M, Saliba M, Vogelgesang R, Giessen H, Alivisatos A P and Liu N 2010 Transition from isolated to collective modes in plasmonic oligomers *Nano Lett.* **10** 2721–6
[35] Fan J A *et al* 2011 DNA-enabled self-assembly of plasmonic nanoclusters *Nano Lett.* **11** 4859–64
[36] Roller E M, Khorashad L K, Fedoruk M and Schreiber R Govorov A O and Liedl T 2015 DNA-assembled nanoparticle rings exhibit electric and magnetic resonances at visible frequencies *Nano Lett.* **15** 1368–73
[37] Li G C, Lei D, Qiu M, Jin W, Lan S and Zayats A V 2021 Light-induced symmetry breaking for enhancing second-harmonic generation from an ultrathin plasmonic nanocavity *Nat. Commun.* **12** 4326
[38] Baumberg J J, Aizpurua J, Mikkelsen M H and Smith D R 2019 Extreme nanophotonics from ultrathin metallic gaps *Nat. Mater.* **18** 668–78
[39] Li G C, Zhang Q, Maier S A and Lei D 2018 Plasmonic particle-on-film nanocavities: a versatile platform for plasmon-enhanced spectroscopy and photochemistry *Nanophotonics* **7** 1865–89
[40] Benz F *et al* 2016 Single-molecule optomechanics in "picocavities" *Science* **354** 726–9
[41] Chikkaraddy R, De Nijs B, Benz F, Barrow S J, Scherman O A, Rosta E, Demetriadou A, Fox P, Hess O and Baumberg J J 2016 Single-molecule strong coupling at room temperature in plasmonic nanocavities *Nature* **535** 127–30
[42] Alù A, Salandrino A and Engheta N 2006 Negative effective permeability and left-handed materials at optical frequencies *Opt. Express* **14** 1557
[43] Yao K and Liu Y 2016 Controlling electric and magnetic resonances for ultracompact nanoantennas with tunable directionality *ACS Photonics* **3** 953–63
[44] Johnson P B and Christy R W 1972 Optical constants of the noble metals *Phys. Rev.* B **6** 4370–9
[45] Li G C, Zhang Y L, Jiang J, Luo Y and Lei D Y 2017 Metal-substrate-mediated plasmon hybridization in a nanoparticle dimer for photoluminescence line-width shrinking and intensity enhancement *ACS Nano* **11** 3067–80
[46] Sobhani A, Manjavacas A, Cao Y, McClain M J, García De Abajo F J, Nordlander P and Halas N J 2015 Pronounced linewidth narrowing of an aluminum nanoparticle plasmon resonance by interaction with an aluminum metallic film *Nano Lett.* **15** 6946–51
[47] Savage K J, Hawkeye M M, Esteban R, Borisov A G, Aizpurua J and Baumberg J J 2012 Revealing the quantum regime in tunnelling plasmonics *Nature* **491** 574–7
[48] Zhu W, Esteban R, Borisov A G, Baumberg J J, Nordlander P, Lezec H J, Aizpurua J and Crozier K B 2016 Quantum mechanical effects in plasmonic structures with subnanometre gaps *Nat. Commun.* **7** 11495
[49] Byers C P, Hoener B S, Chang W S, Link S and Landes C F 2016 Single-particle plasmon voltammetry (spPV) for detecting anion adsorption *Nano Lett.* **16** 2314–21
[50] Chen S *et al* 2018 Plasmon-induced magnetic resonance enhanced Raman spectroscopy *Nano Lett.* **18** 2209–16
[51] Alù A and Engheta N 2008 Dynamical theory of artificial optical magnetism produced by rings of plasmonic nanoparticles *Phys. Rev.* B **78** 085112
[52] Moreau A, Ciracì C, Mock J J, Smith D R, Hill R T, Chilkoti A, Wang Q and Wiley B J 2012

Controlled-reflectance surfaces with film-coupled colloidal nanoantennas *Nature* **492** 86–89
[53] Zambrana-Puyalto X and Bonod N 2015 Purcell factor of spherical mie resonators *Phys. Rev.* B **91** 195422
[54] Brûlé Y, Wiecha P, Cuche A, Paillard V and Colas Des Francs G 2022 Magnetic and electric Purcell factor control through geometry optimization of high index dielectric nanostructures *Opt. Express* **30** 20360
[55] Yang J, Hugonin J P and Lalanne P 2016 Near-to-far field transformations for radiative and guided waves *ACS Photonics* **3** 395–402
[56] Qin F, Zhang Z, Zheng K, Xu Y, Fu S, Wang Y and Qin Y 2022 Transverse Kerker effect for dipole sources *Phys. Rev. Lett.* **128** 193901
[57] Chen W *et al* 2021 Continuous-wave frequency upconversion with a molecular optomechanical nanocavity *Science* **374** 1264–7
[58] Xomalis A, Zheng X, Chikkaraddy R, Koczor-Benda Z, Miele E, Rosta E, Vandenbosch G A E, Martínez A and Baumberg J J 2021 Detecting mid-infrared light by molecular frequency upconversion in dual-wavelength nanoantennas *Science* **374** 1268–71